Thermodynamic Parameters Evaluation of α- and β-cages in Na^+, Ba^{2+}, Fe^{3+}, Co^{2+}, Ni^{2+} and Cu^{2+} Exchanged Zeolite a Using Quantum Mechanical Theory and Fermi Dirac Statistics

[1]Hamida Panezai, [1]Abdul Nabi, [1]Mohammad Yaqoob, [2]Nusrat Munawar, [3]Syed Haider Shah and [4]Syed Mohsin Raza*
[1]*Department of Chemistry, University of Balochistan, Quetta, 87300, Pakistan.*
[2]*Department of Chemistry, Sardar Bahadur Khan Women's University, Quetta, Pakistan.*
[3]*Department of Statistics, University of Balochistan, Quetta, 87300, Pakistan*
[4]*Department of Physics, University of Balochistan, Quetta, 87300, Pakistan.*
smraza7@yahoo.com*

(Received on 7th March 2014, accepted in revised form 27th April 2015)

Summary: The aim of present paper is to investigate the effects of non-framework cations, their hydration capacity and the role of phonons (acoustical and optical) on the thermodynamic characteristics of Type-A zeolite using Quantum mechanical theory and Fermi Dirac Statistics. This study is motivated by the lack of an accurate measurement capability of thermodynamic properties of zeolites by the existing methods reported in literature, that is why we have suggested the quantum mechanical and Fermi Dirac statistical approaches. Thermal analysis data for zeolite samples were obtained by thermogravimetric and differential thermal analysis (TG-DTG) technique at a heating rate of 10 K min^{-1} in order to evaluate the desorption behavior of water. The results showed that the thermal stability of these samples was found to be dependent mainly on the electropositive non-framework cations. Meanwhile, on the basis of thermodynamic parameters, the sizes of α- and β-cages in Na-A and its derivative zeolite were calculated using Fermi Dirac Statistics. Thereafter, semi-quantum effects (logarithmic behavior) of specific heat, entropy and enthalpy were observed in all samples as manifestations of the production of phonons due to gaining of thermal energy. As a result, Debye temperature would increase due to localization of heat energy in the Brillouin zone, and the calculated specific heat capacities showed almost no changes after cation exchange. However entropy and enthalpy first exceeds NaA in Ba^{2+}, Ni^{2+} and Cu^{2+} and then decrease in Fe^{3+} and Co^{2+}. These demonstrations indicated that Ba^{2+}, Ni^{2+}, Cu^{2+} Fe^{3+} and Co^{2+} cations influenced both the entropy and enthalpy as a result of the interaction of cations with the zeolite framework, which confirmed that the changes in the lattice mode were dependent on the increase or decrease in the electrostatic interactions between the cations and the framework zeolite.

Keywords: Zeolite A; TG-DTA technique; Thermodynamic parameters; Quantum mechanical theory; Fermi Dirac statistics; α- and β- cages.

Introduction

Zeolites are crystalline, hydrated aluminosilicates showing an open three dimensional structure consisting of cations needed to balance the electrostatic charge in the framework of silica and alumina tetrahedra. The open structure has made the use of zeolites in several industrial processes such as catalysis, ion exchange and adsorption that are well explained in the literature [1–5].

Sodium A-zeolite is of the cubic symmetry [6]. Rigidly anionic crystalline aluminosilicate framework of synthetic sodium A-zeolite containing α- and β-cavities / cages which have direct access through 8 and 6 oxygen rings, respectively and the 12 Na^+ ions per unit cell (pseudo) are located at three non-equivalent sites in dehydrated zeolites. The intra-crystalline surface area of the dehydrated Type-A zeolite depends on the aspects such as the chemical nature of the cation, location and the thermal stability of the lattice structure [7, 8]. The capacity of changing the composition of a given zeolite e.g. by lattice atom substitution or by introducing metal cations and organic molecules into the pores while maintaining the same crystal structure or contrarily the ability to prepare different crystal structures with the same composition, make them extraordinarily versatile materials with interesting structure-function relationships, which finds many important applications in the energy and chemical processing sectors [9].

The inorganic ion exchangers are superior than organic due to their thermal stability, resistance to radiation and having high selectivity for certain elements [10, 11]. Their selectivity not only depends on the exchanging cations and sorption media but also on the thermal treatment. Therefore, the equilibrium state for both physical and chemical

*To whom all correspondence should be addressed.

systems can be treated quantitatively using thermodynamics. Temperature is a key factor in determining the importance of enthalpy and entropy of a system [10, 11].

According to Hemingway and Robie [1] the best estimation of thermodynamic properties would be achieved from the simultaneous analysis of synthesis and stability data, calorimetric data and different metastable equilibrium measurements. Each of them would place limits upon one or more of the thermodynamic characteristics of a given zeolite phase. Their calculated results of natural phillipsite and clinoptilolite provided valuable information; however, they did not estimate the configuration entropies because of lack of information regarding the degree of order of zeolitic water.

In this case, Tarasevich *et al*. [12] used the direct calorimetric measurements and sorption-analytical method to determine the heats of exchange of the Mn^{2+}, Co^{2+}, Cu^{2+}, and Ni^{2+} cations on the Na^{+} form of clinoptilolite over the entire range of solid phase fillings with sorbed cations.

After that, Greenstein *et al.* [9] investigated the effects of non-framework cations and the role of phonon scattering mechanisms on the thermal transport properties of zeolite LTA using the three-omega method over a wide range of temperature (150–450 K). Overall, previously developed modeling approach derived from semi empirical relaxation time scattering rates along with full anisotropic dispersion, has been further modified and used to calculate the thermal properties of LTA and to analyze its phonon dynamics. This approach provided insight into heat transport in nanoporous materials and has been shown to be transferable to multiple materials. However, accurate predictions of the influences of each type of metal cation on the thermal conductivity of zeolite LTA following mentioned-above methods are rare.

The standard enthalpies (ΔH) and entropies (ΔS) of ion exchange were calculated from isotherms at only two or three temperatures and according to their data analysis the accuracy of the determination of ΔH and ΔS was within measurement errors. For more accurate calculations of the thermodynamic parameters of transition metal exchange using exchange isotherms were made possible by the sorption–analytic method and direct calorimetric measurements of the heats of ion exchange [12]. The accuracy of calculations of thermodynamic characteristics of ion exchanged samples in relation with water content can also be improved by the application of quantum theory and Fermi Dirac Statistics.

The interest in the calculation of the Debye temperature has been increasing in both semi-empirical and theoretical phase diagram calculations since the Debye model offers a simple but very effectual method to explain the phonon contribution to the Gibbs energy of crystalline phases. The energy calculations are often used together with the Debye and Gruneisen model to derive thermo physical properties and phase stabilities at finite temperatures [13]. The quantum mechanical calculations of transition metals exchanged synthetic zeolite-A widely used in investigations has also been studied scantily.

With the aim to further contribute to the knowledge of location and thermal behavior of cations inside zeolites particularly if the zeolitic water content is under consideration with the temperature, this paper provides a deeper investigation of the thermal and structural analysis of the parent Na-A and cation exchanged derivatives: Ba^{2+}, Fe^{3+}, Co^{2+}, Ni^{2+} and Cu^{2+} and a newly developed quantum theory of dielectricity was put forward. The selection of cations has been made to study the implications of size and charge density on ion exchange (their access to the α- and β-cages) and cation-framework interaction.

Experimental

Reagents and Solutions

All plastic ware was cleaned in nutrient free detergent (2%, v/v) (Neutracon, Decon Laboratories, UK), rinsed with ultra-high purity (UHP) water (0.067 μS cm^{-1}, Elga, Purlab Option, UK), soaked overnight in hydrochloric acid (10% v/v), thoroughly rinsed with UHP water and stored in zip-lock plastic bags to avoid contamination. All of the reagents were of analytical grade, supplied by BDH, Fisher Scientific, UK, unless stated otherwise, and all solutions were prepared in UHP water.

Na-A zeolite (70 g, obtained from UOP, USA) was stored over saturated calcium nitrate solution in a desiccator for complete hydration for several days at room temperature. An hydrated fraction (2.5 g) of hydrated NaA zeolite for each sample was taken in 75 mL UHP water and reduced its pH from 11–12 to 7.0 by addition of HCl solution ($1x10^{-3}$ mol L^{-1}). Then 200 mL $FeCl_3.6H_2O$ solution ($5x10^{-3}$ mol L^{-1}) was added at intervals and stirred

for 4 h at 333 K. The slurry was cooled, and then filtered with a fine filter paper.

The exchanged sample was rinsed several times with hot UHP water. The wet samples were dried over night at 353 K in the oven. Partially dehydrated sample was stored again in a desiccator over saturated calcium nitrate to rehydrate for several days. On complete rehydration sample was characterized by thermogravimetric analysis (TGA) and differential thermal analysis (DTA) techniques.

The concentration of the Fe^{3+} ion before and after exchange was analyzed by titration against EDTA solution (0.01 mol L^{-1}) using variamine blue as an indicator till the color changes from blue to yellow. The exchanged concentration of the Fe^{3+} ion in the NaA zeolite was determined by subtracting the concentration of Fe^{3+} ions in the filtrate from the concentration in the original solution.

Out of total 19 samples, 4 samples of Fe^{3+} and Ba^{2+}, 3 samples of Ni^{2+} and Cu^{2+} and 5 samples of Co^{2+} exchanged A-zeolite were prepared by the above procedure. Murexide was used as an indicator for $CuCl_2.2H_2O$, $CoCl_2.6H_2O$ and $NiCl_2.2H_2O$ solutions ($1.7x10^{-2}$ mol L^{-1} each). The color change was observed from greenish yellow to violet in the case of $CuCl_2.2H_2O$ and from yellow to violet in the case of $CoCl_2.6H_2O$ and $NiCl_2.6H_2O$.

During the titration, murexide indicator was used for CoA, NiA, and CuA and Methyl thymol blue for BaA samples [14]. The exact molecular formula for each cation exchanged Na-A zeolite samples are given in Table-1.

Table-1: Summary of cation exchanged Type-A zeolite and percentage of zeolitic water.

S. No.	Sample	Molecular Formula	Percent of zeolitic Water, (%)
01	NaA*	$Na_{12}[(SiO_2)_{12}(AlO_2)_{12}]^{12-}$	30.0
02	1FeA	$Fe_{0.95}Na_{9.2}A$	27.8
03	2FeA	$Fe_{1.85}Na_{6.5}A$	33.1
04	3FeA	$Fe_{2.5}Na_{4.5}A$	34.9
05	4FeA	$Fe_{3}Na_{3}A$	38.6
06	1CoA	$Co_{0.99}Na_{10}A$	39.2
07	2CoA	$Co_{1.965}Na_{8.1}A$	30.7
08	3CoA	$Co_{2.621}Na_{6.8}A$	32.6
09	4CoA	$Co_{3}Na_{6}A$	32.1
10	5CoA	$Co_{3.22}Na_{5.6}A$	33.6
11	1NiA	$Ni_{0.98}Na_{10.04}A$	31.25
12	2NiA	$Ni_{1.9}Na_{8.2}A$	32.56
13	3NiA	$Ni_{3.7}Na_{4.6}A$	35.36
14	1CuA	$Cu_{0.99}Na_{10.02}A$	30.95
15	2CuA	$Cu_{1.96}Na_{8.08}A$	29.45
16	3CuA	$Cu_{2.90}Na_{6.2}A$	31.67
17	1BaA	$Ba_{1}Na_{10}A$	25.9
18	2BaA	$Ba_{1.99}Na_{8.0}A$	26.8
19	3BaA	$Ba_{2.9}Na_{6.2}A$	23.9
20	4BaA	$Ba_{3.8}Na_{4.4}A$	22.3

* represents $[(SiO_2)_{12}(AlO_2)_{12}]^{12-}$

Thermal analysis (TGA, DTA) measurements were carried out for the determination of zeolitic water and thermal characteristics of all zeolite samples using a simultaneous thermal analyzer (STA-40 NETZSCH, Germany). Different weights about 6.50 – 10 mg, for each hydrated samples was taken using high purity nitrogen as purge gas at heating rate of $10^oC\ min^{-1}$ was employed. The content of zeolitic water was calculated by the percent weight loss of samples. The thermal stabilities of the crystal lattices of framework were investigated from exothermic curves of DTA, heated in the temperature range from 30 up to 1000^oC.

Results and Discussion

The percentage of zeolitic water content of hydrated zeolite and its cation exchanged forms were measured by the TGA curves and their summaries are given in Table-1. It shows the zeolitic water content lost per unit cell of hydrated Na-A zeolite is around 30%, comparably, 39% water content per unit cell of hydrated Na-A zeolite was reported by Barrer and Meier [15] and 41% was calculated by Akbar [8]. The standard value of water content is considered to be 37% [16]. The less zeolitic water content in our samples might be due to partial dehydration during the transportation of samples for TGA and DTA analysis. The results (Table-1) showed that the water content per unit cell of the hydrated Fe^{3+}, Ni^{2+}, Co^{2+}, Cu^{2+} and Ba^{2+} exchanged Type A zeolites increased with the increasing number of cations per unit cell of the zeolite. The main reasons might be related to the influence of different cations in cation exchangeable zeolite-A on their pore volume. In general, a small divalent cation increases the void volume by reducing the total number of cations and increasing the space unoccupied [8, 17]. As reported previously [18–20], that exchangeable ions with low charge densities were present in a less hydrated environment and also interacted more strongly with the zeolite framework. Hence, small ions possess a faster access to the internal channels of the zeolite and could easily replace the larger ones. Contrary to this larger, less strongly hydrated cations tended to concentrate in zeolite in contrast to smaller, more hydrated ions, which tended to remain in solution, depending on the type of zeolite. Therefore, the nature of non-framework cations play a key role in water-cation, water-oxygen and water-water interactions [21] and their contribution to the thermodynamic characteristics is significant [22].

The Pauling ionic radii for Co^{2+} and Na^+ ions are 0.74 Å and 0.95 Å [23], respectively,

therefore, the empty space in the cavities increases by exchanging $2Na^{+}$ ions by one Co^{2+} ion. In addition, Co^{2+} ions have the capability of performing complexes with water molecules, in which the water molecules are strongly coordinated to Co^{2+} ions and they are, therefore tightly packed. The zeolitic water content of hydrated Co-A zeolites listed in Table-1 is in good agreement with those obtained by Akbar [8]. Table-1 shows that the water content per unit cell of Ni-A zeolite (Ni^{2+} radius 0.69 Å) is higher than Co^{2+}A-zeolites (Co^{2+} radius 0.74 Å), resulting in a greater hydration ability of Ni^{2+} than that of Co^{2+} in hydrated A zeolite [8, 23], implying a high degree of ordering of water molecules around Ni^{2+} ions .

Furthermore, it has been shown (Table-1) that the increase in the percentage of zeolitic water content per unit cell of Cu^{2+}A zeolite samples is less than Co-A and Ni-A zeolite samples. This might be due to greater ordering of water molecules around Co^{2+} and Ni^{2+} ions as compared to Cu^{2+} ions. John-Teller effect is responsible for the formation of the elongated octahedral (tetragonal) complex of Cu^{2+} in hydrated Cu^{2+}A-zeolites [7]. The percentage water content of Ba^{2+} exchanged Type-A is less as compared to unexchanged NaA and transition metal exchanged samples. It is due to the larger size of Ba^{2+} (1.35 Å) ion and also its inability to form any water complex. These observations on the cation-framework interaction suggested that larger the electropositivity of the non-framework cation lower are the binding energies of the framework element (Si 2p, Al 2p and O 1s) [24], which is in confirmation of our results.

Zeolites skeleton are metastable and are formed by irreversible reactions; consequently, their structures do not exhibit thermodynamic equilibrium with experimental equilibrium and traditional calorimetric procedures. Therefore, their thermodynamic properties cannot be explained properly [25–28]. For the solution of this problem, the newly developed quantum theory of dielectricity [26, 27, 29] was applied. Based on such an idea quantum mechanical and Fermi-Dirac statistical calculations were performed. From the exothermic peaks of DTA curves (Fig. 1a–f) of the NaA zeolite and its cation exchanged samples, the thermodynamic parameters (enthalpy, entropy and specific heat), peak temperature, peak width, transition temperature, Debye velocity, Debye temperature, Debye wave vector, Fermi wave vector were calculated first and corresponding the most important the sizes of α- and β-cages were calculated as listed in Table-2 and -3. The exothermic peaks are in the temperature range from 373K to 1287K.

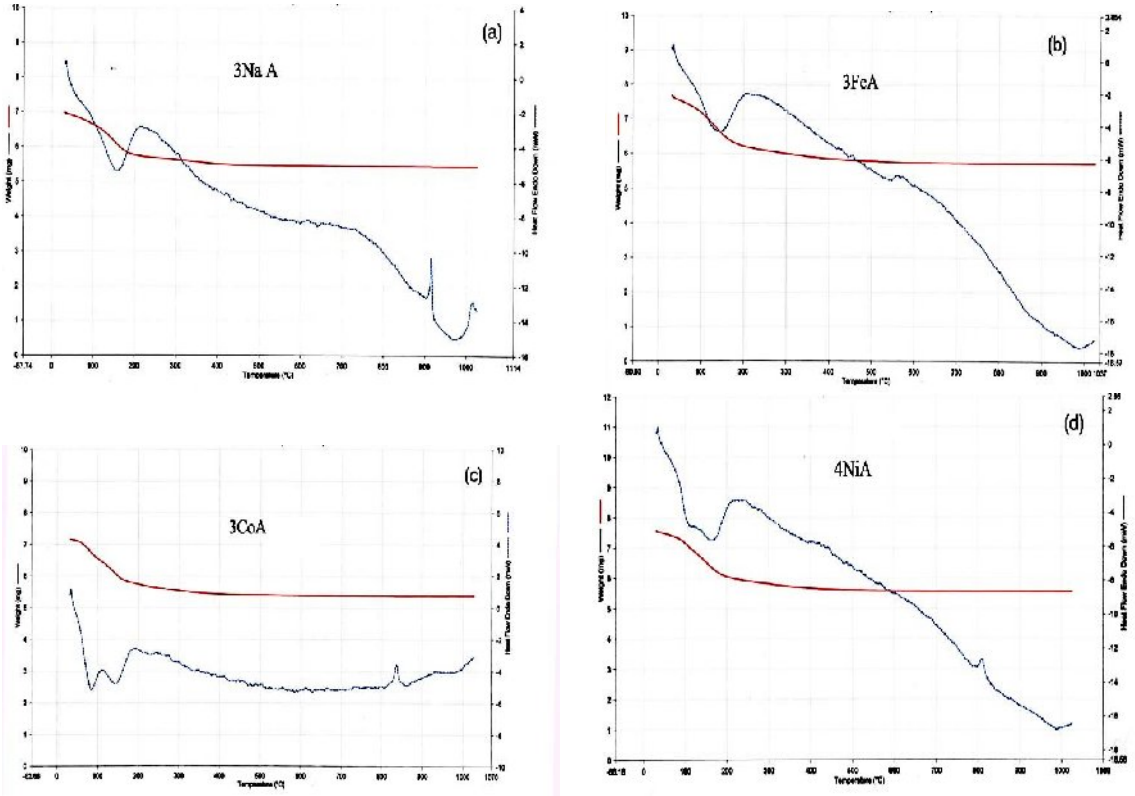

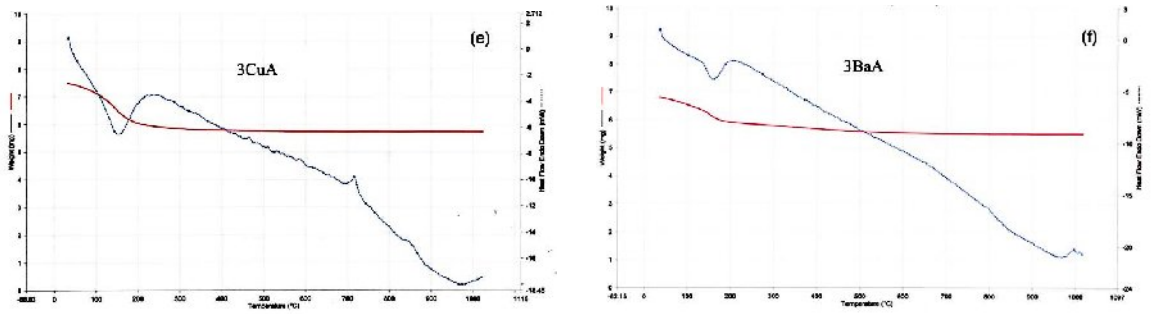

Fig. 1: TGA and DTA profiles for (a) NaA, (b) 3FeA, (c) 3CoA, (d) 3NiA, (e) 3CuA (f) 3BaA zeolites.

Table-2: Results of specific heat, transition temperature, entropy and enthalpy obtained from the exothermic peaks of DTA of both unexchanged and cation exchanged Type-A zeolite.

S. No.	Sample	Peak No	Peak Nature	Mass of Sample (μ Kg)	Specific Heat C (J/KgK)	Peak Temp. Tp (K)	Peak Width □T (K)	Transition Temp Tt(K)	Entropy □S (J/K)	Enthalpy □H (μJ)
01	NaA	01	Exother-mic	7.0	1.13	485	369	T_1=450	6.5	2917
								T_2=558	5.22	
		02			2.89	1185	279		12.5	5619
									10.1	
		03			2.68	1287	282		12.0	5273
									9.5	
02	1NiA	01		7.5	1.13	496	354	T_1=458	7.0	3047
								T_2=565	5.4	
		02			3.00	1220	281		14.0	6319
									11.0	
03	2NiA	01		10	1.20	511	368	T_1=396	11.0	4324
								T_2=654	7.0	
		02			2.05	900	289		15.0	5879
									9.0	
		03			3.10	1253	285		22.0	8834
									13.5	
04	3NiA	01		7.580	1.20	517.4	354	T_1=454	7.0	3185
								T_2=691	5.0	
		02			2.60	1084	280		12.0	5437
									8.0	
05	1CuA	01		8.0	1.13	484	354	T_1=447	7.15	3196
								T_2=721	4.43	
		02			2.72	1135.2	280		14.0	6078
									8.4	
06	2CuA	01		8.0	1.13	493	371	T_1=444	7.65	3396
								T_2=654	5.0	
		02			2.34	1010	287		12.0	5370
									8.20	
		03			3.10	1253	285		16.0	7073
									11.0	
07	3CuA	01		7.505	1.20	500	380.7	T_1=450	7.33	3300
								T_2=638	5.2	
		02			2.30	991	282.24		11.0	4841
									7.6	
08	1BaA	01		8.186	1.13	491.5	351	T_1=462	7.1	3275
								T_2=647	5.1	
09	2BaA	01		7.353	1.13	488.4	369	T_1=462	6.67	3080
								T_2=650	5.0	
		02			2.80	1146	285		12.5	5760
10	3BaA	01		7.0	1.13	480.4	332	T_1=447	6.0	2601
								T_2=821	3.2	
		02			3.14	1265	284		14.0	6259
									7.62	
11	4BaA	01		7.0	1.21	523	354	T_1=496	6.0	2963
								T_2=792	4.0	
12	1FeA	01		7.667	1.20	505	352	T_1=455	7.0	3136
								T_2=698	4.5	
13	2FeA	01		8.0	1.20	502	362	T_1=448	7.5	3355
								T_2=673	5.0	

Table-2 continue

14	**3FeA**	**01**		**7.691**	**1.13**	**484**	**373**	**T_1=444**	**7.3**	**3231**
								T_2=710	**4.55**	
15	**4FeA**	**01**		**7.0**	**1.10**	**473**	**366**	**T_1=419.4**	**7.0**	**2839**
								T_2=687	**4.0**	
16	**1CoA**	**01**	**Exother-mic**	**7.762**	**1.00**	**373**	**292**	**T_1=436**	**5.0**	**2149**
								T_2=629	**3.41**	
		02			**1.13**	**484**	**380**		**7.63**	**3328**
									5.3	
		03			**2.64**	**1115**	**284**		**13.42**	**5853**
									9.30	
17	**2CoA**	**01**		**6.534**	**1.00**	**373**	**291**	**T_1=437.3**	**4.13**	**1805**
								T_2=655	**3.0**	
		02			**1.10**	**462**	**355**		**6.0**	**2529**
									4.0	
		03			**2.60**	**1098**	**284**		**11.02**	**4821**
									7.36	
18	**3CoA**	**01**		**7.167**	**1.00**	**384**	**298**	**T_1=427**	**5.0**	**2062**
								T_2=591	**3.5**	
		02			**1.13**	**490**	**384**		**7.35**	**3134**
									5.30	
		03			**2.64**	**1104**	**285**		**12.55**	**5355**
									9.0	
19	**4CoA**	**01**		**7.399**	**1.00**	**390**	**300**	**T_1=446**	**5.0**	**2165**
								T_2=583	**4.0**	
		02			**1.10**	**463**	**393**		**7.0**	**3173**
									5.44	
		03			**1.21**	**530**	**308**		**6.2**	**2757**
									5.0	
		04			**2.70**	**1130**	**281**		**12.6**	**5612**
									9.62	
20	**5CoA**	**01**		**7.751**	**1.00**	**393**	**288**	**T_1=436**	**5.0**	**2186**
								T_2=573	**4.0**	
		02			**1.10**	**459**	**298**		**6.0**	**2504**
									4.4	
		03			**1.21**	**533**	**314**		**6.8**	**2955**
									5.0	
		04			**2.72**	**1133**	**284**		**14**	**5965**
									10.41	

The exothermic peaks obtained were in the temperature range from 373 K to 1287 K.

Table-3: Results of Debye wave vector, Debye velocity, Debye temperature, sizes of α- and β-cages and Fermi wave vector of unexchanged and cation exchanged Type-A zeolite.

S. No.	Sample	Debye Wave Vector k_D ($x10^9$ m^{-1})	Debye Velocity υ_D ($x10^4$ m sec^{-1})	Debye Temp θ_D (K)	Size of β cage $2\lambda_D$ (nm)	Size of α-cage $2\lambda_F$ (nm)	Fermi Wave Vector k_F ($x10^9$ m^{-1})
1	**Na A**	**14.0**	**2.25**	**2401**	**0.89796**	**1.1326**	**11.10**
2	**1FeA**	**13**	**2.40**	**2401**	**0.9670**	**1.2193**	**10.31**
3	**2FeA**	**13.4**	**2.35**	**2401**	**0.9382**	**1.1849**	**10.61**
4	**3FeA**	**13.7**	**2.29**	**2401**	**0.9176**	**1.1606**	**10.83**
5	**4FeA**	**13.9**	**2.26**	**2401**	**0.9044**	**1.1418**	**11.01**
6	**1CuA**	**12.9**	**2.44**	**2401**	**0.9746**	**1.2325**	**10.2**
7	**2CuA**	**13.11**	**2.40**	**2401**	**0.9589**	**1.2088**	**10.4**
8	**3CuA**	**13.3**	**2.40**	**2401**	**0.9452**	**1.1933**	**10.53**
9	**1NiA**	**12.9**	**2.44**	**2401**	**0.975**	**1.2325**	**10.2**
10	**2NiA**	**13.1**	**2.40**	**2401**	**0.9597**	**1.2088**	**10.4**
11	**3NiA**	**13.5**	**2.33**	**2401**	**0.9312**	**1.1749**	**10.7**
12	**1CoA**	**12.85**	**2.45**	**2401**	**0.9783**	**1.2308**	**10.21**
13	**2CoA**	**13.11**	**2.40**	**2401**	**0.9589**	**1.2088**	**10.4**
14	**3CoA**	**13.23**	**2.38**	**2401**	**0.9502**	**1.1973**	**10.5**
15	**4CoA**	**13.33**	**2.36**	**2401**	**0.9431**	**1.1860**	**10.6**
16	**5CoA**	**13.4**	**2.35**	**2401**	**0.9382**	**1.1860**	**10.6**
17	**1BaA**	**12.8**	**2.50**	**2401**	**0.9821**	**1.2447**	**10.1**
18	**2BaA**	**12.8**	**2.50**	**2401**	**0.9821**	**1.2325**	**10.2**
19	**3BaA**	**12.9**	**2.44**	**2401**	**0.9746**	**1.2205**	**10.3**
20	**4BaA**	**13.0**	**2.42**	**2401**	**0.9670**	**1.2205**	**10.3**

The heat capacity, enthalpy and entropy of Na-A sample are plotted in Fig. 2, and it can be seen that the specific heat was apparently changing linearly with temperature, following the $T^{3/2}$ variation, which could be attributed nearly to Debye specific heat of solids (T^3-variation). This behavior was observed at relatively low temperatures. However, at relatively high temperatures, semi quantum effect (logarithmic behavior) of the specific heat of solids, especially in the proposed case of zeolite, was observed. At 1220K, a peak in NaA was observed, which was due to acoustic phonons only.

The semi-quantum effect (logarithmic behavior) was observed in enthalpy (Fig. 2) and entropy (Fig. 2). The acoustic phonons were produced due to disorder (entropy) in the crystalline phase. This shows that peaks in specific heat or in enthalpy or in entropy were the manifestations of the disorder phenomenon and that these phonons have become free. Phonons were actually quanta of vibrations in the lattices. Vibrations of lattices become pronounced due to gaining thermal energy. The TG curve also illustrates a sharp desorption of water after gaining thermal energy. This confirms the dependence of specific heat capacity, enthalpy and entropy on water content. However Na^+ associated with the framework oxygen proved to be the governing parameter and it can be attributed to the increase in the thermodynamic characteristics of hydrated Na-A sample at transition temperatures to the movement of Na^+ ions provoked by water leaving behind adsorption sites in the framework structure of zeolite, which is found in agreement with the literature [30]. It has also found that there are two types of water present in Na-A zeolite. At low temperatures the weakly attached water (physisorbed) were removed first and at high temperatures as shown in Fig. 1a, the strongly bonded water (chemisorbed) are removed.

Four samples with different concentrations of Fe-exchanged A-zeolite were prepared. It was observed that the relationship of temperature with specific heat was directly and with concentration was inversely proportional. In Fe^{3+} exchanged Type-A zeolites a logarithmic profile ($T^{3/2}$-variation) in the specific heat with curvature at relatively low temperatures, i.e., below about 485 K was observed. The Fe^{3+} ion was ferromagnetic (whether ferrous or ferric). Below 485 K, the optical phonons and at 540K, the acoustical phonons were produced and both were quantized in Brillouin zones. These observations were apparent both in enthalpy and entropy profiles. The shape of such profiles was like Grunession function. However, Fe^{3+} ion shows very different behavior than the other cations (Na^+, Ba^{2+}, Co^{2+}, Cu^{2+} etc). The high polarity of Fe^{3+} ions in zeolites inhibits disorder and maintains crystallinity. Both the optical and the acoustical phonons due to this profile were quantized in Brillouin zones. The temperatures used in our experimental study for iron-exchanged samples of zeolite remain below 510K where the iron ions remain itinerant (Ising model is applicable). The same trends are observed in all its other samples.

Fig. 1e shows TG and DTA profiles of Cu^{2+} exchanged Na-A zeolite. In Cu^{2+} exchanged samples of Na-A, a logarithmic profile ($T^{3/2}$-variation) is observed however, in some cases, a linear trend, for specific heat, enthalpy and entropy (Fig. 4), is also observed with curvatures at relatively high temperatures. The acoustical phonons were produced at above 1000K and were quantized in Brillouin zones. A broad phase transition exothermic curve at maximum temperature of around 505K, showed the heat capacity value in the range 1.13-1.20 J Kg^{-1} K^{-1}. This result is ascertained with the zeolitic water content (30–31%) lost. All the three thermodynamic characteristics were increased and water content was decreased with the increasing temperature.

The profiles of specific heat, entropy and enthalpy (Fig. 5) with logarithmic behavior ($T^{3/2}$ effect) were observed in case of NiA zeolites. The curvatures at relatively high temperatures indicated that acoustical phonons are produced but quantized in Brillouin zones. Ni^{2+} ions in zeolites were ferromagnetic but not polar and itinerant as in the case of Fe^{3+} ions. The specific heat, entropy and enthalpy (thermodynamic characteristics) showed the same increasing trend as seen in Na-A. However, the calculated zeolitic water content (31–35%) was higher than Na-A zeolite, which is attributed to the small ionic radius of Ni^{2+} (0.69 Å) [23].

In the case of cobalt exchanged zeolite samples a crystal clear logarithmic profile ($T^{3/2}$-variation) for specific heat, enthalpy and entropy (Fig. 6) with curvatures at relatively low temperatures is seen. The thermal recovery processes in ion exchanged cobalt samples of zeolites were occurred at about 550K to adjust Brillouin zones, with the exception of Co_4A sample in which optical phonons were generated and became free, whereas in the remaining samples, the acoustical phonons were quantized in Brillouin zones.

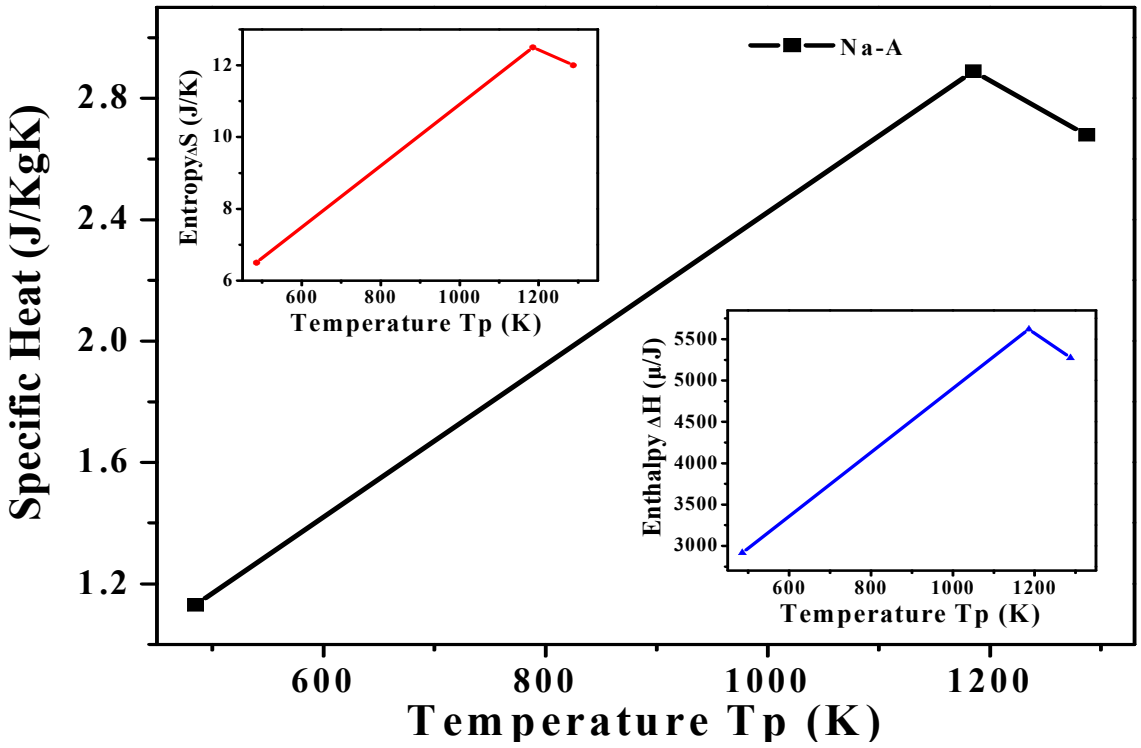

Fig. 2: Effect of temperature on specific heat capacity of Na-A. The inset in the top left panel shows effect of temperature on entropy and inset in the lower right panel shows the effect of temperature on enthalpy of Na-A zeolite.

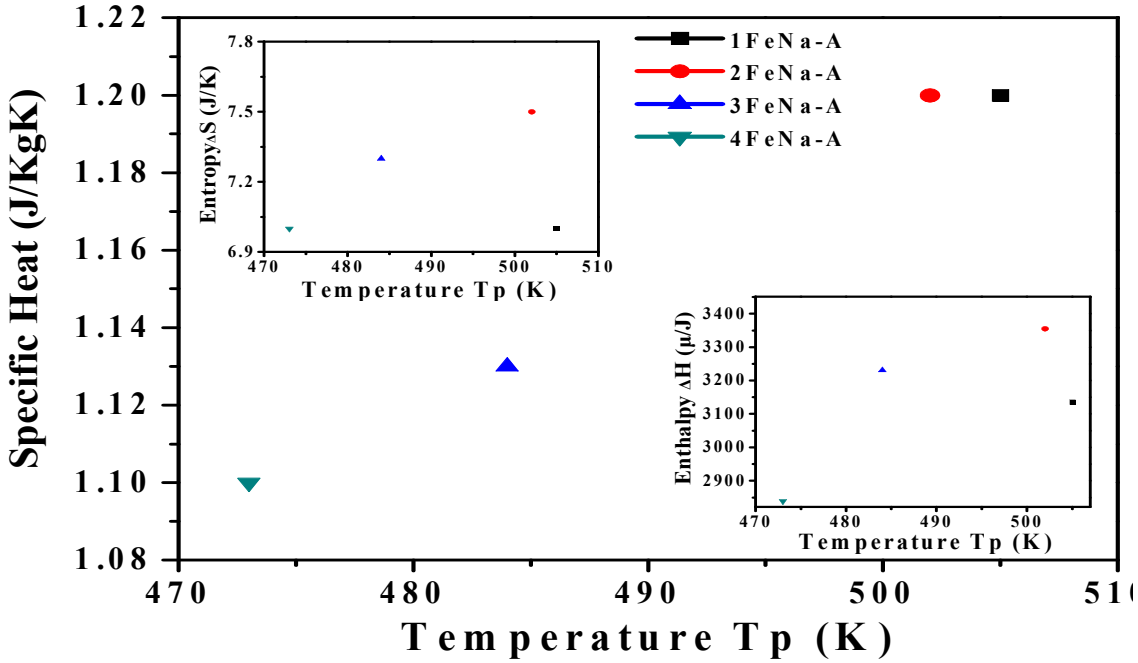

Fig. 3: Effect of temperature on specific heat capacity of different concentrations of Fe, Na-A. The inset in the top left panel shows effect of temperature on entropy and inset in the lower right panel shows the effect of temperature on enthalpy of different concentrations of Fe, Na-A zeolite.

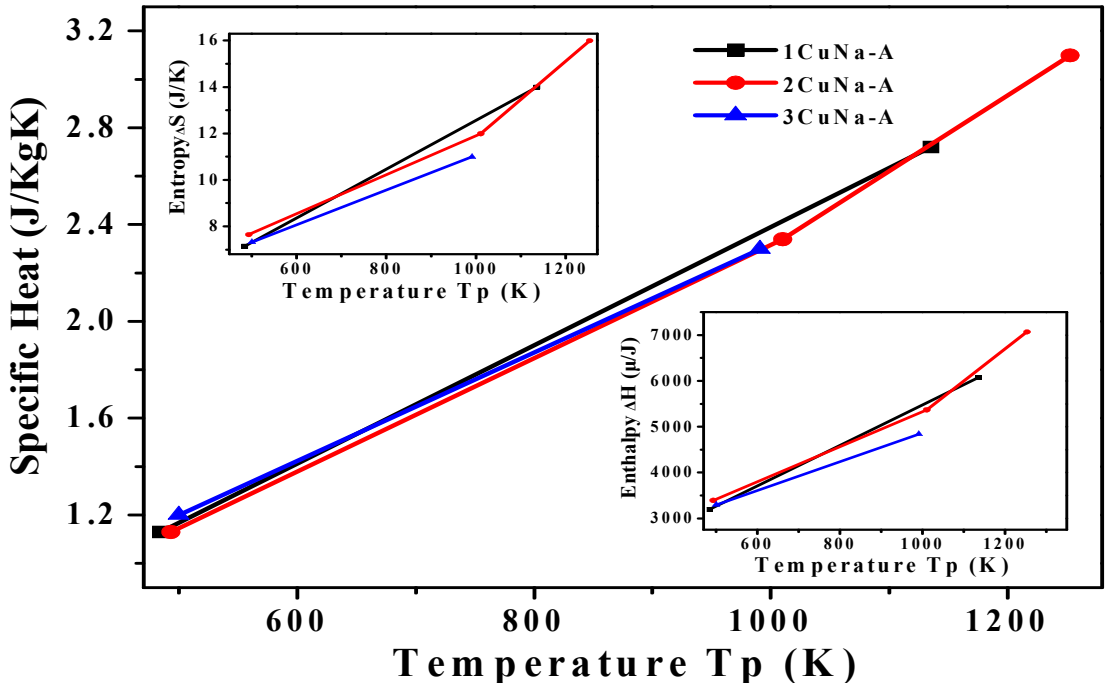

Fig. 4: Effect of temperature on specific heat capacity of different concentrations of Cu, Na-A. The inset in the top left panel shows effect of temperature on entropy and inset in the lower right panel shows the effect of temperature on enthalpy of different concentrations of Cu, Na-A zeolite.

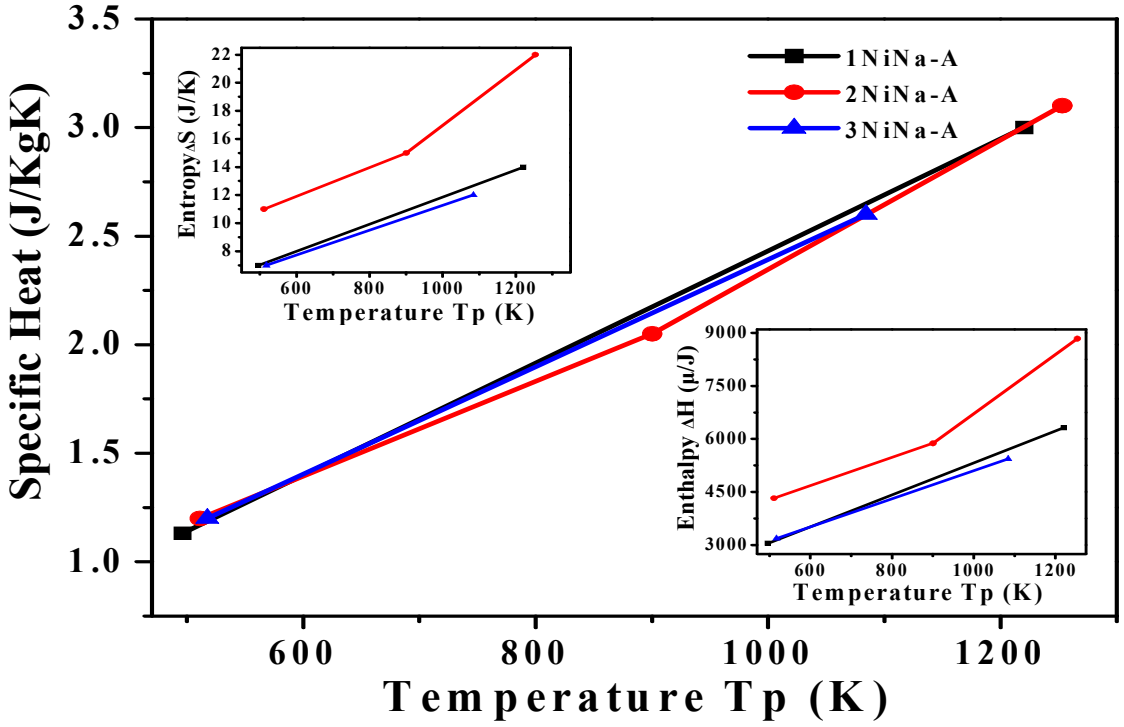

Fig. 5: Effect of temperature on specific heat capacity of different concentrations of Ni, Na-A. The inset in the top left panel shows effect of temperature on entropy and inset in the lower right panel shows the effect of temperature on enthalpy of different concentrations of Ni, Na-A zeolite

In Ba-exchanged Type-A zeolite samples, the specific heat was changing linearly with temperature, following approximately the ($T^{3/2}$- variation), which could be attributed nearly to Debye specific heat of solids (T^3-variation). The shape of the profile associated with specific heat, enthalpy and entropy (Fig. 7) was logarithmic. With increasing concentration of barium, the acoustical phonons were produced with relatively higher energies but were quantized in Brillouin zones. Optical phonons were produced at very high energies or frequencies of lattice vibrations (elastic or super-elastic behavior of lattices). Optical phonons were produced at relatively low temperatures. For Ba^{2+} exchanged samples a less water content as listed in Table-1, in total is observed and this water content showed a decreasing trend with the increasing ion exchange degree, which confirms the weak interaction of Ba^{2+} with water molecules due to its larger size (1.35 Å) [23].

Debye wave vector values decreased from original sample (NaA) towards the cation exchanged samples whereas in ion exchanged samples of same category Debye wave vector values was increased with increasing concentration. It ranges from $14.0x10^9$ m^{-1} to $12.8x10^9$ m^{-1} but the overall Debye wave vector was almost constant for all samples. In contrary, Debye velocity on ion exchange increases and decreased when concentration was increased, because we know that the sound velocity decreases in cage like solid structures. The same behavior was observed in case of all cation exchanged zeolites. Results of Debye wave vector, Debye velocity, Debye temperature, sizes of α- and β-cages and Fermi wave vector of unexchanged and cation exchanged Type-A zeolite samples are given in Table-3. In the case of Cu^{2+} the Debye velocity remains constant in higher concentrations while for Ba^{2+} it remains constant only in the first and second sample.

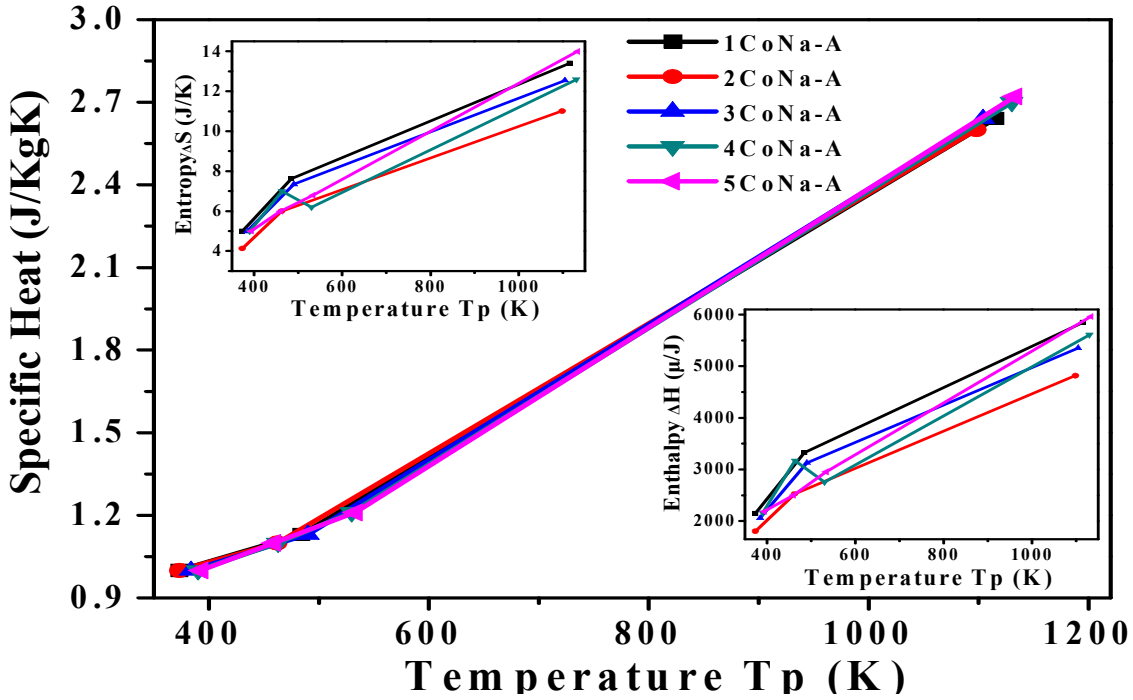

Fig. 6: Effect of temperature on specific heat capacity of different concentrations of Co, Na-A. The inset in the top left panel shows effect of temperature on entropy and inset in the lower right panel shows the effect of temperature on enthalpy of different concentrations of Co, Na-A zeolite.

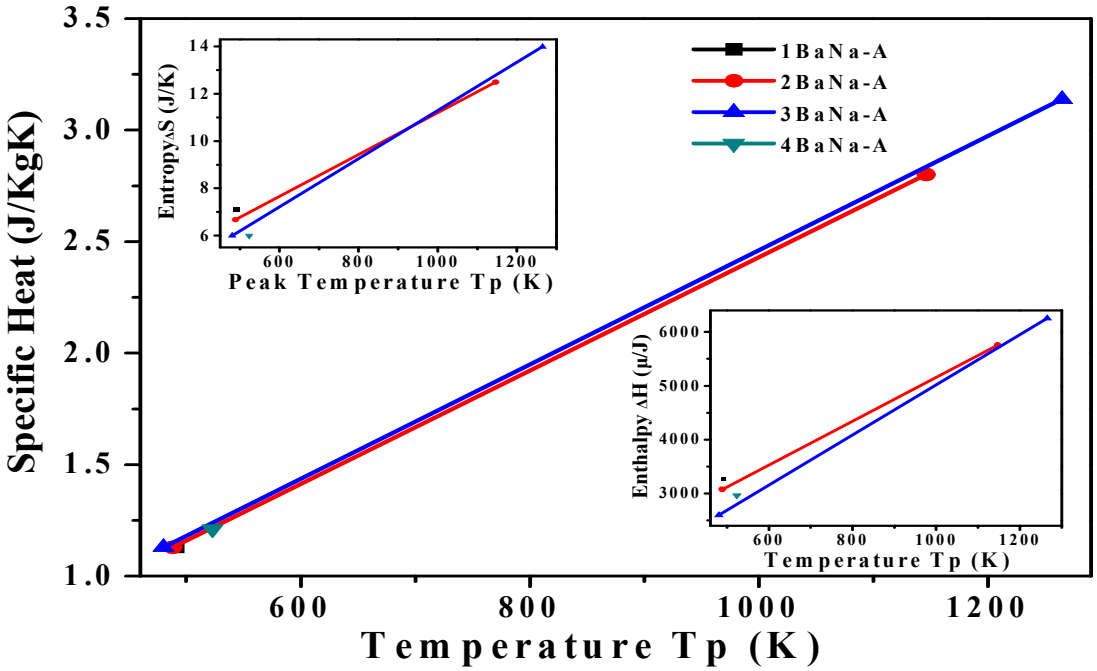

Fig. 7: Effect of temperature on specific heat capacity of different concentrations of Ba, Na-A. The inset in the top left panel shows effect of temperature on entropy and inset in the lower right panel shows the effect of temperature on enthalpy of different concentrations of Ba, Na-A zeolite.

Debye temperature was almost constant in all the samples and its high values (2401K) were because of two reasons, first the structure of zeolite was crystalline and it has already been reported that hard materials exhibit an elevated Debye temperatures and second it behaves as an insulator [31, 32] therefore, the heat energy will be localized in the Brillouin zones, with different modes and in the form high energies. The Brillouin zones could be envisaged like deep quantum wells, the brims of which open up in α- and β-cages. In other words, the channels or pores in zeolites were acting like deep quantum wells.

The total melting point temperature of the three metals Na, Si and Al was almost 2900K that was higher than the 2401K. This justifies the accuracy of the proposed work. The atomic concentration as well as electron concentrations were calculated by employing the formula (N/V) [33], and using well established formulas given in Table-4, Debye wave vector (k_D) and Fermi wave vector (k_F) values were determined and it was found that $k_F < k_D$; as required for a semi disordered system such as amorphous/crystalline or metallic ion exchanged zeolites [34].

Table-4: Formulas of Fermi Dirac Statistics for calculations of Debye wave vector, Debye wave length, Debye velocity, size of β-cage, Debye temperature, Fermi wave vector, Fermi wave length, and size of α-cage.

S. No.	Formula	Unit
1	Debye wave vector $k_D = \left[\frac{6\pi^2 N}{V}\right]^{\frac{1}{3}}$	m^{-1}
2	Debye wave length $\lambda_D = \frac{2\pi}{K_D}$	nm
3	Debye velocity $\upsilon_D = \left[\frac{\omega_D}{6\pi^2 \frac{N}{V}}\right]^{\frac{1}{3}}$	m sec^{-1}
4	Size of β-cage $D_d = 2\lambda_D$	nm
5	Debye temperature $\Theta_D = \frac{\hbar \upsilon_D}{k_B} \left[\frac{6\pi^2 N}{V}\right]^{\frac{1}{3}}$	K
6	Fermi wave vector $k_F = \left[29.60 \frac{N}{V}\right]^{\frac{1}{3}}$	m^{-1}
7	Fermi wavelength $\lambda_F = \frac{2\pi}{k_F}$	nm
8	Size of α-cage $D_F = 2\lambda_F$	nm

We accomplished new findings on the experimental results of Type-A zeolite and its different cations (Fe^{3+}, Cu^{2+}, Ni^{2+}, Co^{2+} and Ba^{2+}) exchanged samples on the basis of quantum mechanical calculations and well established formulas of Fermi Dirac statistics. Particularly, sizes of the cages present in NaA and its ion exchanged forms were calculated using Debye and Fermi wavelengths, respectively.

The results showed that the size of β-cage increases on cation exchange in Type-A zeolite but when the concentration of the cations was increased, making cation exchanged samples of different concentrations; however, the increasing behavior of β-cage is altered. For example in Fe_1A the cage size 0.97 nm was decreased to 0.90 nm in Fe_4A.

The sizes of α-cages show the same increasing trend that of β-cages from NaA zeolite to cation exchanged samples (NaA < FeA < CoA < CuA< NiA < BaA). As the concentration of the cation increased in the NaA-zeolite, the size of the α-cage decreased. It might be due to partial collapse of the crystalline structure of zeolite at high temperature [8]. After 625K (350°C), complete dehydration takes place, due to which the Co^{2+}, Ni^{2+}, Cu^{2+}, Fe^{3+} and Ba^{2+} ions located in the 6-rings made trigonal planar structures with the oxygen. It has already been experimentally proved that the internal surface area of highly exchanged (more than 80%) zeolite Type-A decreased [8] possibly due to partial structure collapse and contraction of the ring size and ultimately the cage size due to energetic vibrations of phonons in the aluminosilicate framework.

Our results for the sizes of both the cages; α-cage is in the range (1.13 – 1.24 nm) and β-cage (0.90 – 0.98 nm) were almost in conformity with those reported in the literature [16]. Debye velocity increases on cation exchange in NaA zeolite depending on the cation nature. Its increasing order is as; NaA < FeA > CuA = NiA < CoA < BaA. But with the increasing cation concentration Debye velocity decreases, because the quantum wells (Brillouin zones) spit cations in the cages, thus becoming shallower. These cations become free ionic bonds (dangling bonds) and were responsible for reducing the sound velocity. To our knowledge it has been the first time that the sizes of cages and channels of zeolite-A have been reported by using Fermi Dirac statistics.

Conclusions

Depending on the size of cation, the zeolitic water content is in the increasing order as Ba < Fe < Na < Cu < Ni < Co. Percentage of zeolitic water loss progressively increased on increasing the cation concentration in FeA, CoA, NiA and CuA zeolite samples, but decreased in BaA zeolite samples depending on the size, nature as well as complex formation ability. The vibrations of lattices become pronounced due to gaining of thermal energy and a logarithmic profile ($T^{3/2}$-variation) for thermodynamic parameters (specific heat, enthalpy and entropy) was observed in all the ion exchanged samples of Type-A zeolite. The heat energy will be localized in the Brilluoin zones, with different modes and high energies, the brims (channels or pores) of which open up in α- and β-cages of zeolites. The calculated wavelengths correlates well to the unit cell parameters and found in agreement with the theoretical prediction for α- and β-cages in Type A zeolites, which further confirm the fact that the development of a cage was the result of the excitation of ions by phonon [26]. Iron is ferromagnetic, polar and remain itinerant, while nickel being ferromagnetic is not polar and itinerant. The sizes of α- and β-cages increase when a small radius cation replaces a large radius cation; contrarily these are decreasing with the increasing concentration of the cation due to two reasons. First it might be due to energetic phonons vibrations in the framework or due to the decreasing Debye velocity. The thermodynamic parameters; specific heat capacity, enthalpy and entropy depend greatly on the temperature as well as on the water content.

Acknowledgments

One of the authors (HP) acknowledges financial support from the higher education Commission, Pakistan (No. 20-1204/R&D/08 2149), and the Department of Education, Provincial Government of Balochistan, for grant of study leave for her PhD degree program and the Department of Chemistry, University of Balochistan for providing research facilities. HP is also thankful to the University of Peshawar for recording thermal analysis curves of the zeolite samples. HP is grateful to Prof. Sher Akber (late) for his intensive co-operation and valuable guidance.

References

1. B. S. Hemingway and R. A. Robie, Thermodynamic Properties of Zeolites; Low-Temperature Heat Capacities and Thermodynamic Functions for Phillipsite and Clinoptilolite; Estimates of the Thermochemical

Properties of Zeolitic Water at Low Temperature, *Am. Mineral*., **69**, 692 (1984).
2. R. M. Barrer, *Zeolites and Clay Minerals as Sorbents and Molecular Sieves*, Academic Press, New York, (1978).
3. R. M. Barrer, Zeolites and their Synthesis, *Zeolites.*, **1**, 130 (1981).
4. J. M. Thomas and W. J. Thomas, *Principles and Practice of Heterogeneous Catalysis*, VCH, New York, p. 515 (1996).
5. J. Weitkamp, Zeolites and Catalysis, *J. Solid State Ionics*., **131**, 175 (2000).
6. P. Demontis, J. G.-Gonzalez, H. Jobic, M. Masia, R. Sale and G. B. Suffritti, Dynamical Properties of Confined Water Nanoclusters: Simulation Study of Hydrated Zeolite NaA: Structural and Vibrational Properties*, ACS Nano.,* **2**, 1603 (2008).
7. S. Akbar, The Dehydration Sequence of Nickel-Exchanged A-Zeolites, *J. Chem. Soc. Pak.,* **4**, 71 (1982).
8. S. Akbar, Ph.D. Thesis, *Structural and Catalytic Aspects of Transition Metals Exchanged A-zeolites*, University of Bradford, (1980).
9. A. Greenstein, Y. Hudiono, S. Graham and S. Nair, Effects of Non-Framework Metal Cations and Phonon Scattering Mechanisms on the Thermal Transport Properties of Polycrystalline Zeolite LTA films, *J. Appl. Phys.*, **107**, 063518 (2010).
10. R. J. Ouellette, *Introductory Chemistry*, Happer and Row Inc, New York, (1970).
11. E. S. Zakaria, I. M. Ali and I. M. El-Naggar, Selectivity and Thermodynamic Characteristics of Doubly Charged Cations on Zirconium Titanate from Aqueous and Alcoholic Solutions, *J. Radioanal.Nucl. Chem.,* **261,** 689 (2004).
12. Y. I. Tarasevich, D. A. Krysenko, V. E. Polyakov and E. V. Aksenenko, The Heats of Exchange of Transition Metal Ions on the Na Form of Clinoptilolite, *Russ. J. Phys. Chem.* A., **82**, 1506 (2008).
13. Q. Chen, and B. Sundman, Calculation of Debye Temperature for Crystalline Structures - A Case Study on Ti, Zr, and Hf, *Acta Mater.,* **49**, 947 (2001).
14. K. M. Dad, M. Phil. Thesis, *Thermodynamic and Infrared Spectroscopic studies of* Cu^{2+}, Ba^{2+}, Ni^{2+}, Fe^{3+} *and* Co^{2+} *Exchanged Synthetic Sodium A-Zeolites*, University of Balochistan, (2001).
15. R. M. Barrer and W. M. Meier, Structural and Ion Sieve Properties of a Synthetic Crystalline Exchanger, *Trans. Faraday Soc.,* **54**, 1074 (1958).
16. W. D. Breck, W. G. Eversole, R. M. Milton, T. B. Reed and T. L. Thomas, Crystalline Zeolite I. The Properties of a New Synthetic Zeolite, Type A, *J.Am. Chem. Soc.*, **78**, 5963 (1956).
17. D. W. Breck, *Zeolite Molecular Sieves, Chemistry and Use*, Wiley-Interscience, New York, (1974).
18. C. Cobzaru, C. Cibotaru, A. Rotariu, A. Marinoiu and S. Oprea, Kinetic Study of the Sorption Process with Cu(II) ions on Clinoptilolite and Analcime: Effects of Temperature and Particle Size, *Chem. Ind. Chem. Eng. Q.,* **15**, 63 (2009).
19. S. Ahmed, S. Chughtai and M. A. Keane, The Removal of Cadmium and Lead from Aqueous Solution by Ion Exchange with Na-Y zeolite, *Sep. Puri. Technol*., **13**, 57 (1998).
20. R. M. Barrer, J. A. Davies and L. V. C. Rees, Thermodynamics and Thermochemistry of Cation Exchange in zeolite Y, *J. Inorg. Nucl. Chem.*, **30**, 3333 (1968).
21. P. Castaldi, L. Santona, C. Cozza, V. Giuliano, C. Abbruzzese, V. Nastro and P. Melis, Thermal and Spectroscopic Studies of Zeolites Exchanged with Metal Cations, *J. Mol. Struct.*, **734,** 99 (2005).
22. G. K. Johnson, H. E. Flotow, P. A. G. O'Hare and W. S. Wise, Thermodynamic studies of zeolites: Natrolite, Msolite, and Scolecite, *American Mineralogist.*, **68**, 1134 (1983).
23. F. A. Cotton and G. Wilkinson, *Advanced Inorganic Chemistry*, Wiley-Interscience, New York, (1972).
24. M. Huang, A. Adnot and S. Kaliaguine, Cation-Framework Interaction in Alkali-Cation-Exchanged Zeolites: an XPS study, *J. Am. Chem. Soc.*, **114**, 10005 (1992).
25. W. E. Jr. Dibble and W. A. Tiller, Kinetic Model of Zeolite Paragenesis in Tuffaceous Sediments, *Clay. Clay Miner.*, **29**, 323 (1981).
26. B. S. Hemingway, *Advances in Physical Geochemistry*, Springer-Verlag, New York, p. 285 (1982).
27. S. Jabeen, S. M. Raza, M. A. Ahmed, M. Yaseenzai, S. Akbar and Y. Z. Jafri, Quantum Mechanical Analysis on Faujasite-Type Molecular Sieves by Using Fermi Dirac Statistics and Quantum Theory of Dielectricity, *J. Chem. Soc. Pak.,* **34**, 251 (2012).
28. S. M. M. R. Naqvi, S. D. H. Rizvi, S. M. Raza, S. Rizvi, A. Hussain and F. Rehman, An Estimation of Enthalphy of Amorphons Alloys Using Differential Thermal Analysis, *J. Chem. Soc. Pak.,* **24**, 1 (2002).
29. S. Jabeen, S. M. Raza, K. Mehmood, S. Atiq and Z. Farooqi, Analysis of Dolomite of Balochistan (Pakistan) by Using X-Ray Fluorescence Spectroscopy (XFS), Simultaneous Differential

Thermal Analysis (SDTA), Thermogravimetric Analysis (TGA) and Differential Scanning Calorimetry (DSC), *J. Chem. Soc. Pak.*, **31**, 1 (2009).

30. M. M. Mohamed, Heat Capacities, Phase Transitions and Structural Properties of Cation Exchanged H-Mordenite Zeolite, *Thermochim. Acta*., **372**, 75 (2001).
31. A. Djedid, S. Mec-abih, O. Abbes and B. Abbar, Theoretical Investigations of Structural, Electronic and Thermal Properties of Ti 2AlX(X=C,N), *Physica. B.,* **404**, 3475 (2009).
32. C. R. A. Catlow, R. A. van Santen and B. Smit, *Computer Modelling of Microporous Materials*, Elsevier, p. 165 (2004).
33. C. Kittel, *Introduction to Solid State Physics*, Wiley, New York, p. 21 (2005).
34. M. A. Gormani, S. M. Raza, N. Farooqui, M. A. Ahmed, and T. Abbas, On Thermally Activated Electrical-Resistivity in Metallic Glasses, *Sol. State Commun.*, **95**, 329 (1995).